Supporting Information

Controlled Assembly and Plasmonic Properties of Asymmetric Core-Satellite Nanoassemblies

*Jun Hee Yoon, Jonghui Lim, and Sangwoon Yoon**

Department of Chemistry, Institute of Nanosensor and Biotechnology, Dankook University

152 Jukjeon-ro, Suji-gu, Yongin

Gyeonggi 448-701

Korea

Phone: +82-31-8005-3152

Fax: +82-31-8005-3148

E-mail: sangwoon@dankook.ac.kr

1. Synthesis and Characterization of Nanoparticles

Materials. The following compounds were purchased and used as received: gold(III) chloride trihydrate (Aldrich, $HAuCl_4 \cdot 3H_2O$, ≥ 99.9%), sodium citrate tribasic dehydrate (Aldrich, $C_6H_9Na_3O_9$, ≥ 99.0%), (3-aminopropyl)trimethoxysilane (Aldrich, $C_6H_{17}NO_3Si$, 97%), 1,2-ehanedithiol (Aldrich, $C_2H_6S_2$, ≥ 90%), 1,4-butanedithiol (Aldrich, $C_4H_{10}S_2$, 97%), 1,6-haxanedithiol (Aldrich, $C_6H_{14}S_2$, 96%), 1,8-octanedithiol (Aldrich, $C_8H_{18}S_2$, ≥ 97%), 1,10-decanedithiol (TCI, $C_{10}H_{22}S_2$), 1,16-hexadecanedithiol (Aldrich, $C_{16}H_{34}S_2$, 99%), benzyl mercaptan (Aldrich, 99%), RBS detergent solution (Fluka, 35 concentrate), ethanol (Duksan, ≥ 99.9%), acetonitrile (Duksan, ≥ 99.5%), THF (Duksan, ≥ 99.5%), hexane (Duksan, ≥ 95.0%), water (J. T. Baker, HPLC grade), and citrate-capped silver nanoparticles (diameters ~ 50 nm, Ted Pella).

Synthesis of nanoparticles. For the synthesis of the 13 nm AuNPs, we employed the citrate reduction method developed by Turkevich and coworkers.[1] A solution of sodium citrate (340 mM, 5 mL) was added to a boiling solution of $HAuCl_4$ (0.254 mM, 995 mL) with vigorous stirring. Continuous heating for 30 min changed the color of the solution to red. The final solution has a maximum extinction at 522 nm with a molar extinction coefficient of 2.07×10^8 $M^{-1}cm^{-1}$. The TEM images showed that the AuNPs have a diameter of 12.6 ± 0.8 nm (Figure S1).

We modified the previously reported seeded growth method to prepare 7.4, 18, 22, 32, 47, and 51 nm AuNPs.[2] The reaction conditions and results are summarized in Table S1. The seeds for the 7.4 nm AuNPs were synthesized by adding an aqueous solution of $NaBH_4$ (74 mM, 1 mL) to a 100 mL mixture solution of $HAuCl_4$ (0.25 mM) and sodium citrate (0.60 mM). The size of the seed particles was 2.8 ± 0.6 nm. The seeds for the 47 and 51 nm AuNPs were prepared by the reduction of $HAuCl_4$ (25 mM, 1 mL) using sodium citrate (2.2 mM, 150 mL) and measured at 16.3 ± 1.4 and 18.5 ± 1.7 nm, respectively. For the other sizes of AuNPs, the 13 nm AuNPs were used as seeds.

For the growth of the seed particles, stock solutions of $HAuCl_4$ (25 mM) and sodium citrate (60 mM) were prepared. Then, the following volumes of solution were consecutively added to the seed solution and reacted for different periods of time at 85 °C, given in Table S1. The sizes of the synthesized AuNPs were determined by TEM (Figure S1). The maximum extinction wavelength and the calculated molar extinction coefficient of each AuNP are also presented in Table S1.

AgNPs were synthesized by reduction of $AgNO_3$ using citrate. A solution of sodium citrate (160 mM, 20 mL) and a solution of $AgNO_3$ (50 mM, 20 mL) were mixed in 950 mL of deionized water. Very small

amounts of $NaBH_4$ (0.4 mM, 10 mL) were added for the size control and the mixture was brought to reflux for 3 h. The product AgNPs have a diameter of 12.7 ± 2.7 nm and the maximum extinction at 393 nm (Figure S1). For the assembly, the final solution was diluted by a factor of four. The 50 nm AgNPs for the core in the assembly were purchased (Ted Pella) and used after dilution by a factor of two.

Table S1. The reaction conditions and the results of the seeded growth method for the AuNP synthesis.

Unit: mL unless otherwise noted.

		Rxn Time	**7.4 nm**	**18 nm**	**22 nm**	**32 nm**	**47 nm**	**51 nm**
Seed	Size		2.8 nm	13 nm	13 nm	13 nm	16 nm	19 nm
	Volume		101	700	300	200	151	151
1st growth	Water				200	50		
	Citrate	5 min	1.00	5.10	4.60	3.00		
	$HAuCl_4$	35 min	0.50	5.10	2.30	1.50	1.00	1.00
	$HAuCl_4$	35 min	0.50		2.30	1.50	1.00	1.00
	Water		100		200	150	150	148
2nd growth	Citrate	5 min	2.00	7.00	9.56	9.60	5.57	5.56
	$HAuCl_4$	35 min	1.00	3.50	4.78	3.20	2.79	2.78
	$HAuCl_4$	35 min	1.00	3.50	4.78	3.20	2.79	2.78
	$HAuCl_4$	35 min				3.20		
	Water		300	276	272	200	300	300
3rd growth	Citrate	5 min	4.00			10.20	11.42	11.33
	$HAuCl_4$	35 min	2.00			3.40	5.67	5.67
	$HAuCl_4$	35 min	2.00			3.40	5.67	5.67
	$HAuCl_4$	35 min				3.40		
	Water		485			355	363	365
Diameter (nm)			7.4 ± 1.2	17.9 ± 1.1	22.2 ± 1.3	31.7 ± 3.3	47.4 ± 4.3	50.5 ± 6.0
λ_{max} (nm)			518	521	521	527	531	532
ε_{max} (10^9 M^{-1} cm^{-1})			0.04	0.70	1.4	4.5	16	19

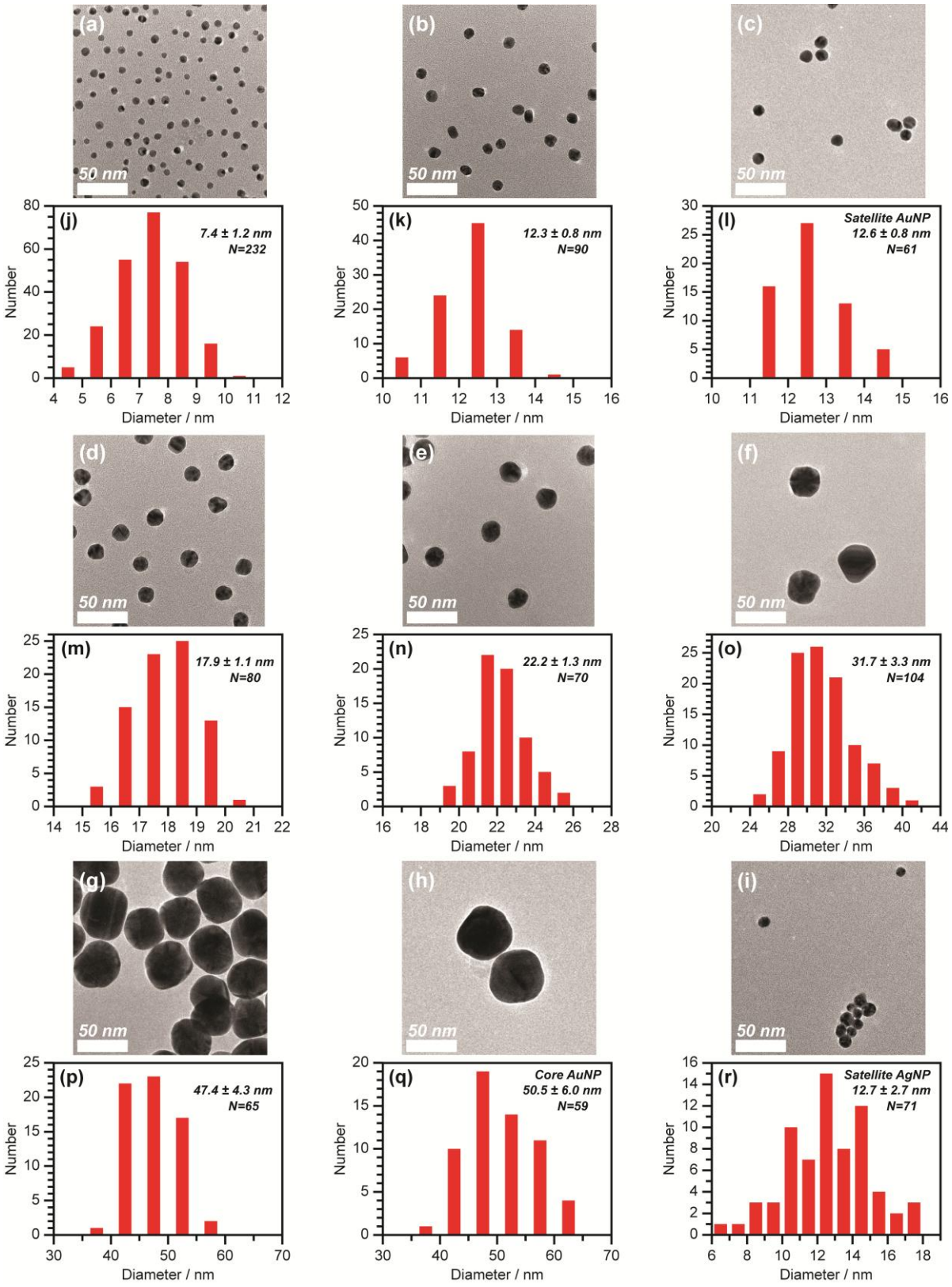

Figure S1. TEM images and size distributions of the synthesized AuNPs and AgNPs.

2. Scalability of the Assembly Method

One potential problem with the new assembly method we present is scalability. Because our method is based on the desorption of nanoparticles from glass substrates, the area of the glass substrates limits the number of assemblies. The number of asymmetric core-satellite nanoassemblies prepared from a 25 mm × 12 mm glass slide in our experiments was 1.7×10^{10} or 5.6 pM in 5 mL of ethanol. Although this concentration of nanoassemblies is good enough to study fundamental plasmonic properties such as surface plasmon coupling and SERS, as presented in the manuscript, higher concentrations are often required for other applications. Here, we present how we measured the number of nanoassemblies and discuss how we can scale up the quantities.

2.1 Quantification of the number of nanoassemblies produced from one glass slide

The number of nanoassemblies is determined by the number of core AuNPs (51 nm) adsorbed on the glass substrate in step 2 of the assembly process because the core AuNPs are completely desorbed into solution in step 5 after their surfaces are covered with the satellites (Figure 3h). We can quantify the number of core AuNPs adsorbed on the glass substrate by measuring the decrease in the extinction of the core AuNP solution after the immersion of the glass substrates. Figure S2 shows that the extinction of the core AuNP solution decreases from 0.60 to 0.49 (18% decrease) when the amine-coated glass substrate is immersed in the core AuNP solution (27 pM, 5 mL) for 12 h, as described in the manuscript. From the molar extinction coefficient of the core AuNPs (51 nm), $\varepsilon_{max} = 1.9 \times 10^{10}$ $M^{-1}cm^{-1}$,[3] and Beer's law, the number of adsorbed core AuNPs (and thus the number of nanoassemblies) is determined to be 1.7×10^{10}.

The yield of the assemblies is 100%, as determined from the number of core AuNPs that *lead to* the assembly product out of the core AuNPs that *react* with the satellites; this is because it is the core AuNPs on the substrates that react with the satellites in step 4 and all the core AuNPs come out as the assemblies. From a different perspective, however, if the yield of the assemblies is defined as the ratio of the number of produced nanoassemblies to the total number of core AuNPs used for the entire process, regardless of whether they are introduced to the reaction with satellites or not, then it will be 18% as determined above.

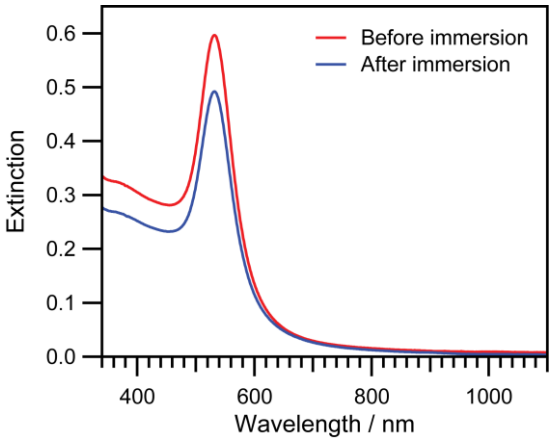

Figure S2. UV–vis spectra of the 51 nm AuNP solution before (red) and after (blue) immersion of the amine-coated glass substrate (25 mm × 12 mm) for 12 h.

2.2 Scale-up of the production of nanoassemblies

We can conceive of two possible methods to increase the concentration of the sample, maintaining all the advantages of our assembly scheme. The simplest way is obviously to use more glass slides or a larger glass slide. We tested this idea by desorbing the asymmetric core-satellite nanoassemblies from ten glass slides repeatedly in 5 mL of ethanol solution. Figure S3a shows the contrast in color between the nanoassembly solutions from one glass slide (left) and ten glass slides (right). The comparison of the UV–vis spectra between the two in Figure S3b clearly shows that the concentration increased by a factor of ten. The exact overlap in the spectral shape without any new bands in the long wavelength region indicates that the nanoassemblies remained stable and did not aggregate at this concentration.

The other scale-up method we are currently pursuing is to use magnetic silica particles (MSPs). Taking advantage of the enormously large surface areas of microparticles for a given volume, we can drastically increase the number of nanoassemblies desorbed from the silica particles. Figure S4 illustrates the concept of increasing the number of asymmetric core-satellite nanoassemblies using MSPs. The assembly process using MSPs is fundamentally the same as the process using glass substrates. One complication is that both the nanoassemblies and MSPs will coexist as dispersions in solution after the selective desorption of the nanoassemblies by sonication. However, the magnetic core of the MSPs will allow us to separate the desorbed nanoassemblies from the silica particles.

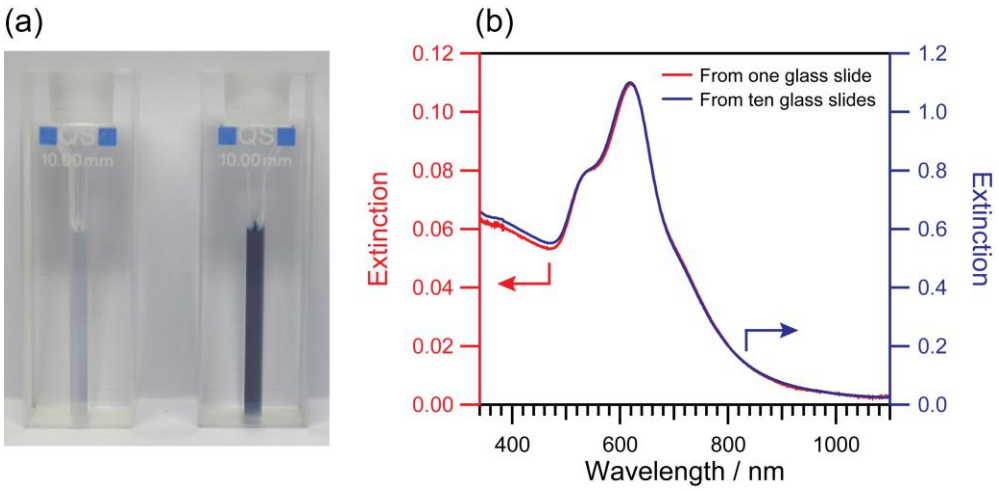

Figure S3. (a) Color and (b) UV–vis spectra of the asymmetric core-satellite nanoassemblies prepared using one glass slide (left cuvette, red spectrum) and ten glass slides (right cuvette, blue spectrum) in ethanol.

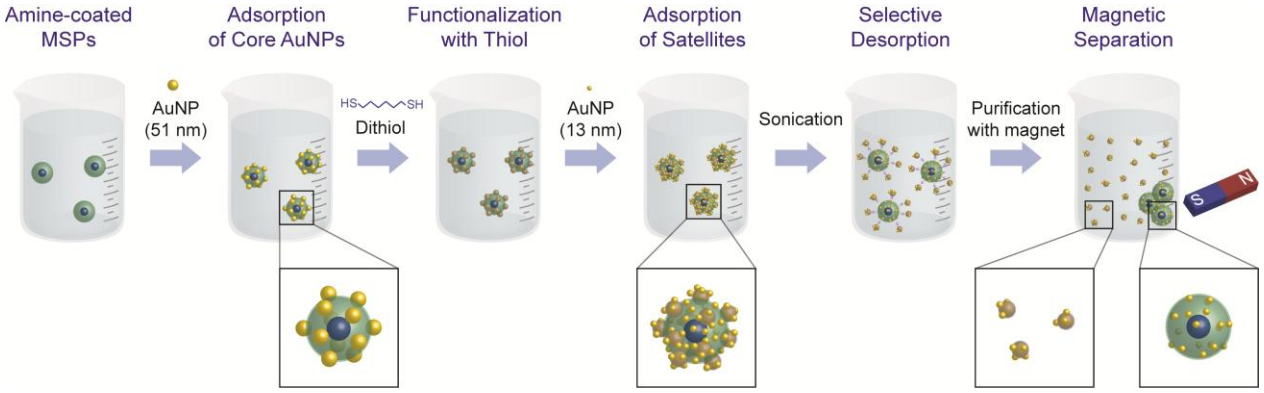

Figure S4. Scheme of large-scale production of asymmetric core-satellite nanoassemblies using magnetic silica microparticles.

The scale-up of the nanoassemblies using the above scheme is currently in progress in our laboratory. To test the feasibility of this idea, we performed preliminary experiments using regular (not magnetic) silica microparticles (diameter ~ 750 nm). Figure S5 presents the scanning electron microscopy (SEM) images of the silica microparticles after the formation of core-satellite AuNP assemblies on the surfaces and ensuing sonication. The results show that the formation of the core-satellite nanoassemblies and

their selective desorption upon sonication occur on silica microparticles exactly in the same fashion as on glass substrates, strongly suggesting that this scheme is highly feasible.

Furthermore, MSPs are commercially available (usually for biological applications) in bulk quantities. For example, MoBiTec (http://www.mobitec.de), based in Germany, provides amine-functionalized MSPs (diameter ~ 1 μm) in 2, 10, and 100 mL volumes at a concentration of 3–9 × 10^9 / mL. The use of 5 mL of such MSPs has the same effect on the surface area as more than 100 sheets of glass slides. Therefore, we can scale up the quantities of asymmetric core-satellite nanoassemblies using MSPs.

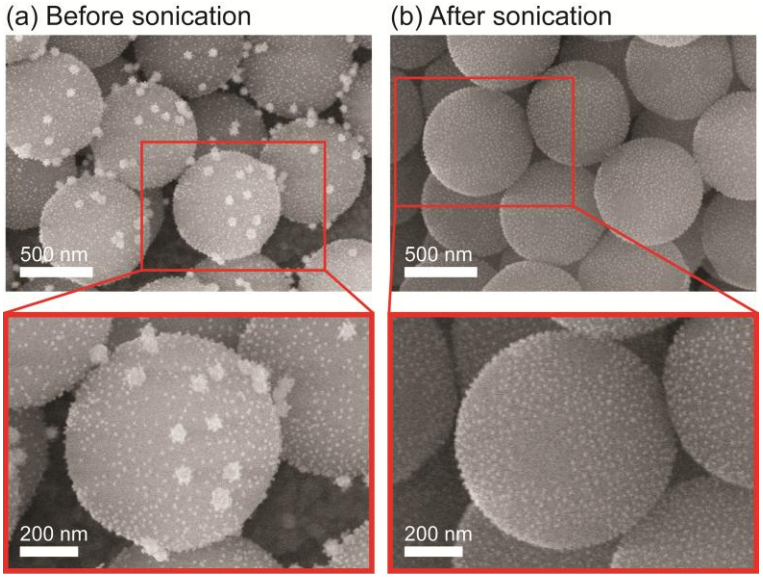

Figure S5. SEM images of silica microparticles (a) after the formation of core-satellite AuNP assemblies on the surfaces, following the scheme in Figure S4, and (b) after subsequent sonication.

3. Additional TEM and Ultrahigh Resolution SEM Images of Asymmetric Core-Satellite Nanoassemblies

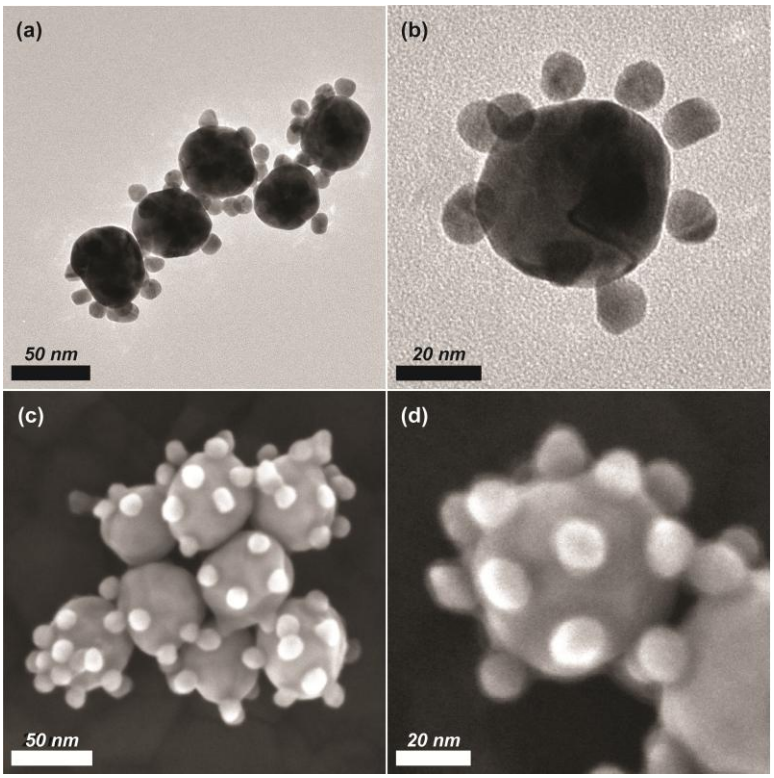

Figure S6. TEM (upper panels) and UHR SEM (lower panels) images of the asymmetric core-satellite nanoassemblies of AuNPs. DDT was used as a linker between the core and the satellites.

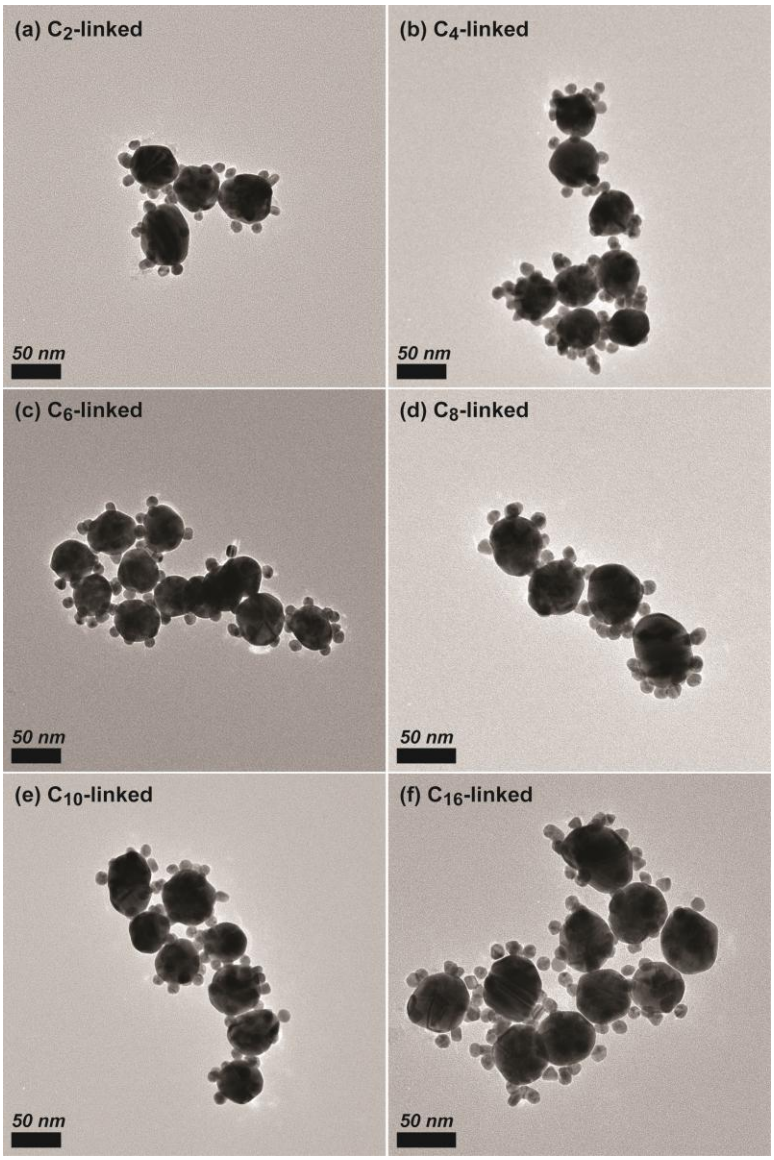

Figure S7. TEM images of the asymmetric core-satellite nanoassemblies of AuNPs in which the core and the satellites are linked by (a) 1,2-ethanedithiol, (b) 1,4-butanedithiol, (c) 1,6-hexanedithiol, (d) 1,8-octanedithiol, (e) 1,10-decanedithiol, or (f) 1,16-hexadecanedithiol.

4. Calculations of Interparticle Distances

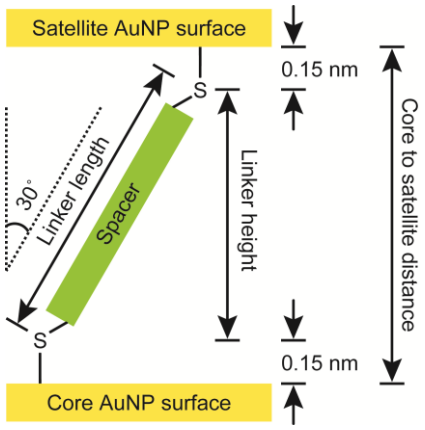

Figure S8. Schematic illustration of the core-to-satellite interparticle distance, defined by the self-assembled monolayers of alkanedithiol.

Table S2. Calculated lengths of the alkanedithiol linkers and converted core-to-satellite surface-to-surface interparticle distances.

Unit: nm

	Linker length	Linker height	Core-to-satellite distance
C2	0.443	0.383	0.683
C4	0.691	0.599	0.899
C2 dimer	0.859	0.744	1.044
C6	0.944	0.818	1.118
C8	1.199	1.038	1.338
C10	1.454	1.260	1.560
C16	2.222	1.924	2.224

C2: 1,2-ethanedithiol, C4: 1,4-butanedithiol, C2 dimer: dimeric form of C2 (2-mercaptoethyl disulfide), C6: 1,6-hexanedithiol, C8: 1,8-octanedithiol, C10: 1,10-decanedithiol, C16: 1,16-hexadecanedithiol.

The interparticle distance between the core and the satellite is determined by the thickness of the self-assembled monolayer (SAM) of alkanedithiol formed on the core surfaces. Contrary to the most commonly known alkanethiol SAMs, studies of alkane*di*thiol SAMs are rare. Frisbie and coworkers reported that atomic force microscopy (AFM) and X-ray photoelectron spectroscopy (XPS) studies show

that the alkanedithiol SAMs have analogous structures to the alkanethiol SAMs, but there is a wide spread in the thickness values.[4] Our attempts to measure the thickness of a series of alkanedithiol SAMs using ellipsometry have also yielded inconsistent and irreproducible values. Transmission electron microscopy (TEM) should be the most judicious choice of technique for directly measuring gap distances. However, in this study, the variations in the interparticle gap distance of two methylene groups are in the range of 2–3 Å. It is almost impossible to discern such small interparticle distances reliably by TEM.

Due to the lack of reliable experimental data, we calculated the thickness of the alkanedithiol SAMs using density functional theory (DFT). The dithiol molecules adsorb onto gold surfaces *via* the formation of Au–S bonds.[5] Van der Waals interchain interactions induce the formation of SAMs with an upright orientation, tilted by 30° (Figure S8).[4-8] The lengths of the alkanedithiol molecules were calculated using *Gaussian 03* [B3LYP/6-311G(d,p)], and the results are presented in the second column of Table S2.[9] Taking the tilt angle (30°) and the distance from the Au surface to S (1.5 Å) into account yields the core-satellite interparticle gap distances.[10]

The validity of our calculations has been checked. First, we performed similar calculations for alkanethiol (R–SH) SAMs because alkanethiol SAMs are very well known and have been more extensively studied. Our calculation result for decanethiol SAMs (1.36 nm) was consistent with previous experimental (1.31 nm)[11] and theoretical (1.36 nm)[12] values. The second piece of evidence that supports the validity of our calculations is the comparison between our calculation results and any known experimental values for dithiol SAMs. One experimental data available is the thickness of 1,2-ethanedithiol SAMs measured by ellipsometry.[10] The calculated interparticle distance (0.68 nm), as defined in Figure S8, is in excellent agreement with the experimental value of the 1,2-ethanedithiol SAMs (0.65 nm), considering that the S–Au bond is slightly longer than the S–H bond. Therefore, we believe that our calculations provide reasonable values for the interparticle distances.

5. Influence of Bilayer Formation Kinetics of 1,2-ethanedithiol on Surface Plasmon Coupling

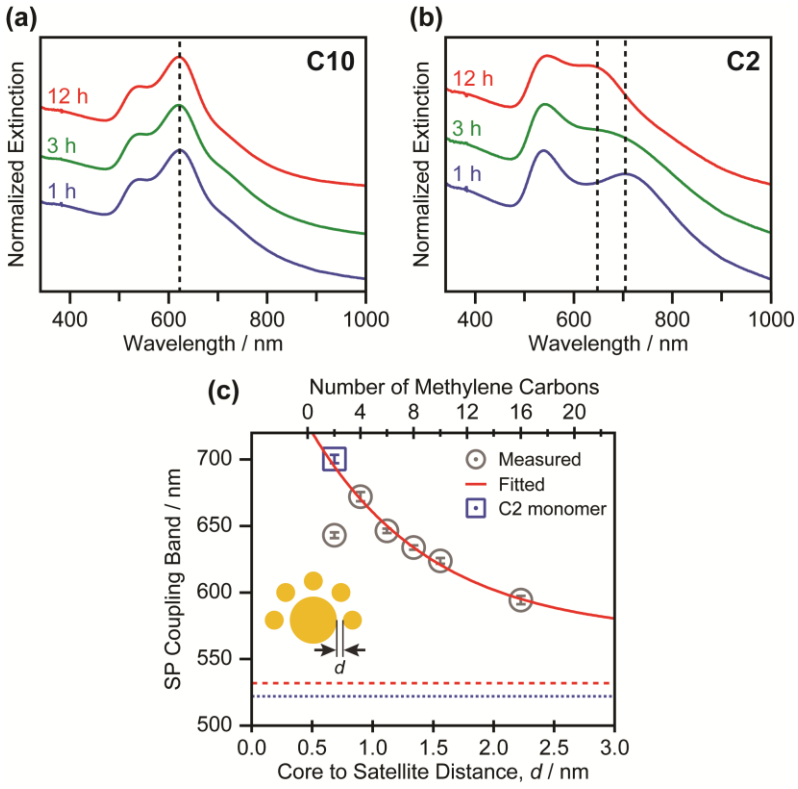

Figure S9. UV–vis spectra of the asymmetric core-satellite nanoassemblies linked by (a) 1,10-decaneditiol and (b) 1,2-ethanedithiol. The indicated times are the immersion times in step 3 of the assembly process, allowing the SAMs of the corresponding linkers to form on the core AuNP surfaces. The dashed lines are visual guides to show the changes of the surface plasmon coupling bands. (c) A plot of the measured surface plasmon coupling wavelengths as a function of the core-to-satellite gap distances (circles). The red line is an exponential function fitted to the data from C4 to C16. A blue square mark the surface plasmon coupling wavelength of the C2-linked nanoassemblies with the immersion time of 1 h (701 nm).

The surface plasmon coupling wavelength of the core-satellite nanoassemblies linked by 1,2-ethanedithiol (C2) apparently does not follow the trend of red-shifts with shorter interparticle distances, as shown in Figure 6 in the main text. We attribute this anomaly to the bilayer formation of C2 on the core AuNP surfaces *via* disulfide bond.[10] The length of the disulfide form of C2 is comparable with the

length of C6. Therefore, the surface plasmon coupling band of C2 appears at a wavelength similar to that of C6, strongly supporting our interpretation.

Another piece of evidence comes from the kinetic study. We shortened the time for the formation of SAMs on the core AuNPs to 1 and 3 h from 12 h so that the bilayer formation of C2 is less likely [Step 3 of the assemble process in Figure 3]. As a control, we performed the same experiments for C10 linkers.

Figure S9 presents the UV–vis spectra of the resulting core-satellite nanoassemblies for the C10 and C2 linkers. Both spectra show the strong surface plasmon coupling bands. However, while the surface plasmon coupling band of the C10-linked core-satellites does not depend on the SAM formation time, that of the C2-linked core-satellites changes from 701 nm to 649 nm as the time extends. SAMs start to form within an hour upon the immersion of gold surfaces into thiol solutions although the formation of a more stable and robust structure takes > 12 h.[5] Such a quick formation of SAMs, followed by their stabilization, is reflected in the unchanged surface plasmon coupling wavelength for the C10-linked core-satellites (Figure S9a). The interparticle distance between the core and the satellites for these nanoassemblies is maintained by the formation of C10 SAMs. In contrast, the change of the surface plasmon coupling band for the C2-linked core-satellites suggests that the height of the SAMs on the core AuNP surfaces changes with the reaction time. We believe that a short period of time (1 h) allows for only the formation of monolayers of C2, causing a strong surface plasmon coupling between the core and the satellites at 701 nm. With a longer time (12 h), C2 bilayers are formed on the core AuNPs, yielding a weaker surface plasmon coupling that is comparable with the coupling of AuNPs by C6 monolayers. The observed time scale of the bilayer formation of C2 is also consistent with the result from the ellipsometry measurements by Kim and coworkers, where they found that it takes ~2 h for C2 to form a bilayer on Au in ethanol.[10] In contrast, Linford and coworkers reported that it takes a few days for hexanedithiol (C6) to form bilayers.[8] Furthermore, the surface plasmon coupling band at 701 nm from the interparticle distance defined by the C2 monolayers (square in Figure S9c) falls right on the fitting curve (red line), strongly supporting our interpretation.

6. Calculation of SERS Enhancement Factors

The SERS enhancement factor (EF) is defined by the Raman scattering intensity of a molecule in the presence of nanoparticles relative to that of the molecule in the absence of nanoparticles. Thus, the EF is expressed as follows:

$$EF = \frac{I_{sample} / N_{sample}}{I_{ref} / N_{ref}},$$

where I / N indicates the Raman intensity per molecule. The "sample" is the benzyl mercaptan (BM) molecules in this case, residing in the SERS hot spots of the asymmetric core-satellite nanoassemblies that produce the SERS signal; the "reference" is the BM molecules in solution that provide the normal Raman spectrum without any SERS effects.

Because we acquired the Raman spectra for both the sample and reference in Figure 7c under the same conditions, we can directly compare the Raman intensities from the spectra. The number of BM molecules in the reference (N_{ref}) is obtained from the concentration of the solution (0.1 M, 5 mL) used for a normal Raman spectrum. To estimate the number of BM molecules in the SERS hot spots, we assumed that the hot spots are formed in the junction between the core and the satellites.[13] Then, from the area of the SERS hot spot defined by the diameter of the satellites (13 ± 1 nm), the adsorption area of thiol on Au (0.2 nm^2),[14] the number of satellites per an assembly (13 ± 3), and 4:1 mixed SAMs of C10 and BM on the core surfaces, we determined the number of BM molecules in the hot spot per assembly to be 1700 ± 700 [= π $(13 / 2)^2$ nm^2 × 13 / 0.2 nm^2 × (1/5)]. Considering the number of assemblies in 5 mL of ethanol (four times concentrated), the total number of BM in the SERS hot spots (N_{sample}) is (1.2 ± 0.5) × 10^{14} or 39 ± 16 nM. Therefore, from the above equation, the SERS EF is (1.6 ± 0.7) × 10^6.

7. Drying Effect

The aggregation of nanoparticles on the glass substrates upon drying is evident from the comparison of the UV–vis spectra taken with the sample immersed in solution with those of the dried sample. We acquired the UV–vis spectra for two sets of AuNP-adsorbed substrates. One sample was kept in solution, and UV–vis spectra were also taken with the sample in the solution. The other sample was dried in air, as prepared for SEM measurements. We compared each spectrum with the UV–vis spectrum of the colloidal AuNPs dispersed in aqueous solution to monitor the states of the AuNPs on the glass substrate. Figure S10 shows that the core AuNPs, both citrate-capped and functionalized with DDT from step 2 and step 3 of the assembly process, respectively, remain well dispersed on the glass substrate as long as the AuNP-adsorbed substrate is in solution. It is when the solvent completely dries that the AuNPs become aggregated, as indicated by the new extinction bands at longer wavelengths. These results clearly indicate that the aggregation is caused by the drying effect and the AuNPs remain well dispersed on the substrate in solution.

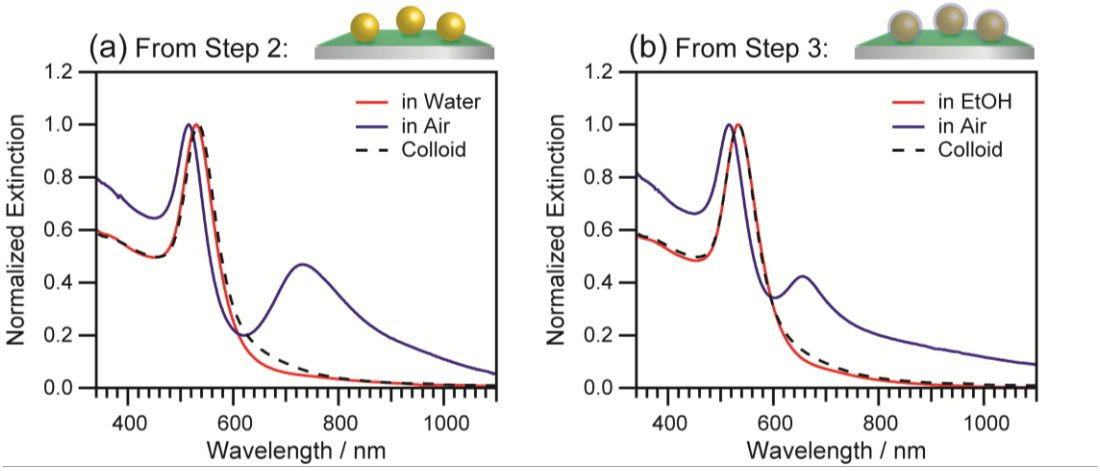

Figure S10. UV–vis spectra of (a) the core AuNP-adsorbed glass substrate from step 2 of the assembly process, and (b) the core AuNP-adsorbed glass substrate after being immersed in DDT solution for 12 h (step 3 of the assembly process). Red and blue lines indicate the spectra acquired from the sample kept in solution and in air, respectively. We have included the UV–vis spectra of the core AuNPs dispersed in solution for comparison (dashed lines).

References

(1) Turkevich, J.; Stevenson, P. C.; Hillier, J. A Study of the Nucleation and Growth Processes in the Synthesis of Colloidal Gold. *Discuss. Faraday Soc.* **1951**, *11*, 55–75.

(2) Bastús, N. G.; Comenge, J.; Puntes, V. Kinetically Controlled Seeded Growth Synthesis of Citrate-Stabilized Gold Nanoparticles of up to 200 nm: Size Focusing *versus* Ostwald Ripening. *Langmuir* **2011**, *27*, 11098–11105.

(3) Liu, X.; Atwater, M.; Wang, J.; Huo, Q. Extinction Coefficient of Gold Nanoparticles with Different Sizes and Different Capping Ligands. *Colloids Surf., B* **2007**, *58*, 3–7.

(4) Engelkes, V. B.; Beebe, J. M.; Frisbie, C. D. Length-Dependent Transport in Molecular Junctions Based on SAMs of Alkanethiols and Alkanedithiols: Effect of Metal Work Function and Applied Bias on Tunneling Efficiency and Contact Resistance. *J. Am. Chem. Soc.* **2004**, *126*, 14287–14296.

(5) Love, J. C.; Estroff, L. A.; Kriebel, J. K.; Nuzzo, R. G.; Whitesides, G. M. Self-Assembled Monolayers of Thiolates on Metals as a Form of Nanotechnology. *Chem. Rev.* **2005**, *105*, 1103–1169.

(6) Rieley, H.; Kendall, G. K.; Zemicael, F. W.; Smith, T. L.; Yang, S. X-Ray Studies of Self-Assembled Monolayers on Coinage Metals. 1. Alignment and Photooxidation in 1,8-Octanedithiol and 1-Octanethiol on Au. *Langmuir* **1998**, *14*, 5147–5153.

(7) Raya, D. G.; Madueño, R.; Blázquez, M.; Pineda, T. Formation of a 1,8-Octanedithiol Self-Assembled Monolayer on Au(111) Prepared in a Lyotropic Liquid-Crystalline Medium. *Langmuir* **2010**, *26*, 11790–11796.

(8) Madaan, N.; Terry, A.; Harb, J.; Davis, R. C.; Schlaad, H.; Linford, M. R. Thiol-Ene-Thiol Photofunctionalization of Thiolated Monolayers with Polybutadiene and Functional Thiols, Including Thiolated DNA. *J. Phys. Chem. C* **2011**, *115*, 22931–22938.

(9) Gaussian 03, Revision C02, 2004, Wallingford, CT.

(10) Joo, S. W.; Han, S. W.; Kim, K. Multilayer Formation of 1,2-Ethanedithiol on Gold: Surface-Enhanced Raman Scattering and Ellipsometry Study. *Langmuir* **2000**, *16*, 5391–5396.

(11) Bain, C. D.; Troughton, E. B.; Tao, Y. T.; Evall, J.; Whitesides, G. M.; Nuzzo, R. G. Formation of Monolayer Films by the Spontaneous Assembly of Organic Thiols from Solution onto Gold. *J. Am. Chem. Soc.* **1989**, *111*, 321–335.

(12) Liang, J.; Rosa, L. G.; Scoles, G. Nanostructuring, Imaging and Molecular Manipulation of Dithiol Monolayers on Au(111) Surfaces by Atomic Force Microscopy. *J. Phys. Chem. C* **2007**, *111*, 17275–17284.

(13) Wustholz, K. L.; Henry, A.-I.; McMahon, J. M.; Freeman, R. G.; Valley, N.; Piotti, M. E.; Natan, M. J.; Schatz, G. C.; Van Duyne, R. P. Structure-Activity Relationships in Gold Nanoparticle Dimers and Trimers for Surface-Enhanced Raman Spectroscopy. *J. Am. Chem. Soc.* **2010**, *132*, 10903–10910.

(14) Mohri, N.; Inoue, M.; Ara, Y.; Yoshikawa, K. Kinetic Study of Monolayer Formation with 4-Aminobenzenethiol on a Gold Surface. *Langmuir* **1995**, *11*, 1612–1616.